Ocean Engineering 279 (2023) 114507

Contents lists available at ScienceDirect

Ocean Engineering

journal homepage: www.elsevier.com/locate/oceaneng

A rectified unidirectional rotary PTO for two-body wave energy converters

Saeed Rezaei [a,*], Amir Rahimi [a], Jamshid Parvizian [a], Shahriar Mansoorzadeh [b], Alexander Düster [c]

[a] Department of Mechanical Engineering, Isfahan University of Technology, Isfahan, 84156-83111, Iran
[b] Research Institute for Subsea Science & Technology, Isfahan University of Technology, Isfahan, 84156-83111, Iran
[c] Institute for Ship Structural Design and Analysis, Hamburg University of Technology (TUHH), Am Schwarzenberg-Campus 4 C, D-21073, Hamburg, Germany

ARTICLE INFO

Handling Editor: Prof. A.I. Incecik

Keywords:
Wave energy converter
Point absorber
Unidirectional rotational motion
PTO

ABSTRACT

This work presents a new mechanism for a mechanical power take-off (PTO) system that can be used in a variety of wave energy converters (WECs). This mechanism uses two ball screws to convert the relative linear motion of the WEC bodies into unidirectional rotary motion. The resulting rotary motion finally causes a generator to rotate and generate electricity. Due to the oscillatory nature of the wave, the relative velocity of the WEC bodies will have a sinusoidal motion; therefore, the angular velocity of the ball screw becomes zero at two moments during one period of movement. The designed mechanism prevents the generator shaft from changing its direction of rotation at these moments. This mechanism also decouples the generator shaft from the ball screw when the angular velocity of the generator shaft exceeds the angular velocity of the ball screw due to its rotational moment of inertia. As the relative velocity of the bodies increases, the generator shaft is re-coupled to the ball screw and, in consequence, rotates at the angular velocity of the ball screw. This article examines the effect of using the present mechanism on increasing the electrical output power of the WEC at different wave frequencies.

1. Introduction

The high potential renewable energy of ocean waves has attracted remarkable attention to various possibilities of harvesting electricity from sea waves. Many countries have invested in developing WECs as a solution to overcome the fuel crises as well as global warming. Despite many scientific efforts to evolve the WECs, the technology of energy harvesting from sea waves is still immature. Therefore, more effort is needed to achieve a real breakthrough. Generally speaking, WECs can be classified into three categories based on their working principles: (i) oscillating water column (OWC), (ii) overtopping systems, and (iii) oscillating bodies (Falcão, 2010). The first and the second category are suitable for inshore and nearshore locations, respectively. For the far offshore areas, which provide higher wave energy density compared to the areas close to the shore, the third category is more suitable (Morim et al., 2014; Illesinghe et al., 2017).

Point absorbers (PAs) are oscillating body systems whose dimensions, with respect to wavelengths, are relatively small. They are able to harvest energy from movements in all directions (Falnes, 2007; Al et al., 2019a, 2019b). PAs usually have one or two bodies to harvest energy from waves, as well as a power take-off (PTO) system to convert and transmit the captured energy.

The foci of research on PAs are (i) to determine the hydrodynamic coefficients to develop accurate mathematical models (Falnes, 1999; Zurkinden et al., 2014; Pastor and Liu, 2014; Beatty et al., 2015; Liang and Zuo, 2017; Miquel et al., 2017), (ii) to optimize the shape and dimensions to increase the ability of capturing energy (Kurniawan and Moan, 2012; Goggins and Finnegan, 2014; Wen et al., 2018; Al et al., 2019a, 2019b), (iii) to present control algorithms to achieve the optimal conditions (Babarit and Clement, 2006; Babarit et al., 2009; Wu et al., 2018; Zhang et al., 2014), and (iv) to develop the PTO in order to enhance the energy conversion (Bozzi et al., 2013; Liang et al., 2017; Li et al., 2020; Yang et al., 2021). For all types of WECs, the PTO system is one of the most important components, as it directly affects the dynamics of a WEC. Therefore, the reliability, performance, efficiency, cost, and maintenance of a PTO are important factors that must be considered. Two common types of PTOs used in PAs are hydraulic drive systems (Henderson, 2006; António, 2007; Cargo et al., 2012) and direct-drive linear electric generators (Khatri and Wang, 2020; Polinder et al., 2007; Prudell et al., 2010; Hodgins et al., 2011). The hydraulic systems usually consist of an oil piston pump, a gas accumulator, and a rotational electric generator. Despite the high energy loss in the tubes,

* Corresponding author.
E-mail address: Rezaei.sr@me.iut.ac.ir (S. Rezaei).

https://doi.org/10.1016/j.oceaneng.2023.114507
Received 3 October 2022; Received in revised form 17 March 2023; Accepted 7 April 2023

the low efficiency of the hydraulic PTO, fluctuations in the output power, and despite being bulky, heavy, and relatively expensive, hydraulic PTOs have been used in some pilot projects like Aquabuoy (Weinstein et al., 2004), Pelamis (Henderson, 2006), WaveRoller (Folley et al., 2007), and Wavebob (Weber et al., 2009).

Direct-drive linear generators consist of a translator magnetic and a coil. They are suitable for low-velocity wave oscillations. Thanks to the lack of mechanical friction, there is no considerable loss of energy. However, this system requires heavy magnets. Further, the output power is bidirectional and highly fluctuating. These generators have been used in Lysekil (Leijon et al., 2008) and Oregon State University buoys (Brekken et al., 2009).

Liang et al. (2017) proposed a new PTO system called *mechanical motion rectifier* (MMR). This PTO converts linear motion into rotational motion, using a rack-and-pinion mechanism. It benefits from one-way bearings to rectify the rotational motion. A similar concept is introduced by Li et al. (2020). They designed and analyzed a PTO with a ball screw, as the motion converter, and a compact MMR gearbox. The MMR gearbox uses one-way bearings and bevel gears to rectify the rotation – and a detachable flywheel to decrease the speed fluctuation of the generator by increasing the equivalent mass of the engaged system. Yang et al. (2021) proposed a coaxial MMR with a variable inertia flywheel (VIF). These kinds of PTOs have been used in single-body PAs.

The current study presents a new mechanism for the rotational PTO which acts on a two-body WEC. The WEC geometry is adopted from Powerbuoy PB500, and its dimensions are optimized to absorb the maximum power. The hydrodynamic coefficients of the WEC and the wave forces acting on the buoy are calculated and determined by numerical and experimental methods. The size optimizing process and hydrodynamic coefficients extraction of the WEC are fully described in (Rezaei et al., 2022; Rahimi et al., 2022), respectively, prepared by the current authors. The WEC geometry and its dimensions are shown in Fig. 1. The linear and rotational PTO systems used in two-body WECs follow the relative velocity of the WEC bodies created by wave oscillations. The oscillation of ocean waves can be approximated by a sinusoidal motion. In each wave period, there are two turning points where the relative direction of motion of the WEC bodies starts to change and the linear relative velocity becomes zero. Since the PTO and the generator obey the movement of the bodies, the direction of the generator rotation, consequently, has to change at each turning point as well. Therefore, part of the kinetic energy of the WEC must be spent on overcoming the rotational moment of inertia of the generator shaft, in order to change its rotational direction at each turning point. In this paper, we present a novel PTO mechanism that prevents energy dissipation due to a change of relative linear motion direction of a two-body point absorber WEC. This mechanism converts the otherwise bi-directional motion of the generator shaft into a unidirectional and rectified rotational motion. The specifically designed mechanism also keeps the generator's velocity from becoming zero. This means that the generator follows the relative motion of the bodies at a certain part of the oscillating period and, when the relative velocity of the bodies becomes zero, the generator continues to rotate freely due to its inertia. This causes the generator to rotate continuously in one direction, without stopping.

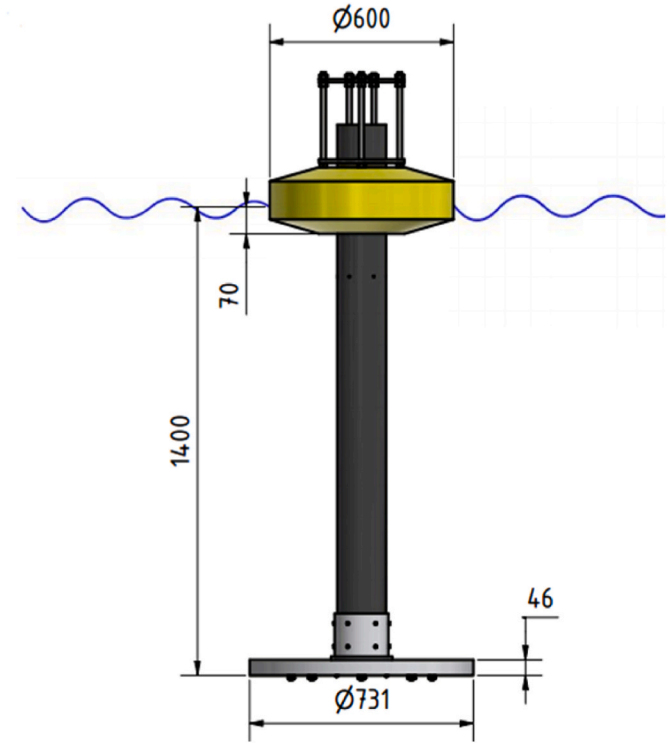

Fig. 1. General dimensions of the studied WEC (Rezaei et al., 2022).

The structure of this paper is as follows. In Section 2, the mechanism of the rectified unidirectional PTO is presented in detail. The dynamic equations of the mechanism as well as the equation of the motion of the two-body WEC are given in Section 3. The absorbed power and optimal conditions for both bidirectional and rectified unidirectional PTOs are the subjects of Section 4. Section 5 presents the results and compares the performance of bidirectional and rectified PTOs. Section 6 concludes the paper.

2. Design of the PTO

Since sea waves are of an irregular nature – and since incoming waves include a range of frequencies – the optimal conditions for the harvesting parameters cannot be achieved with specific PTO fixed parameters. Therefore, this paper addresses this problem with a new PTO design. This PTO includes a DC rotary generator and a directional rectifier. With this mechanism, the direction of rotation of the generator will be independent of the direction of movement of the buoys. Optimal conditions can be obtained by adjusting the external resistance of the generator. Fig. 2 depicts this PTO. The special feature of this PTO is the rectification of the axis of rotation of the generator shaft. A ball-screw mechanism is used to convert the linear motion of the floating and submerged body of the primary converter to the rotational motion of the generator shaft. Rotational direction rectification is obtained using one-way bearings together with an intermediate gear coupled to the shaft of the generator. Unlike the bi-directional mechanisms in which the system's inertia causes energy dissipation when the direction of vertical reciprocal motion changes, there is no such dissipation in this specifically designed mechanism, as the direction of rotation of the generator shaft axis does not change. When the direction of movement of the buoys changes, the moment of inertia causes the shaft of the generator continues to rotate. In this case, the rotational speed of the generator axis is greater than the rotational speed of the ball screw. This causes the gear coupled to the generator to disengage from the ball screw gear. The gears are then re-engaged as the ball screw speeds up. Therefore, the equations of motion of the buoys only include the PTO force at the time of the gear engagement.

Fig. 2 shows the mechanical parts of the PTO-design, which is installed inside a two-body wave energy converter consisting of a floating and a submerged body. The rods (A) are connected to the floating body, while the other parts of the PTO are connected to the submerged body. The relative motion of the two bodies causes the rods (A) and, consequently, the ball screw nuts (D) to linearly move up and down. The ball screw nuts (D) move along ball screws (B and C). Since the ball screws are restrained at both ends by the deep groove ball bearings (J), the linear motion of the nuts is finally converted to the rotational motion of the ball screws. The ball screws are mechanically identical, except for the fact that one is left-handed and the other is

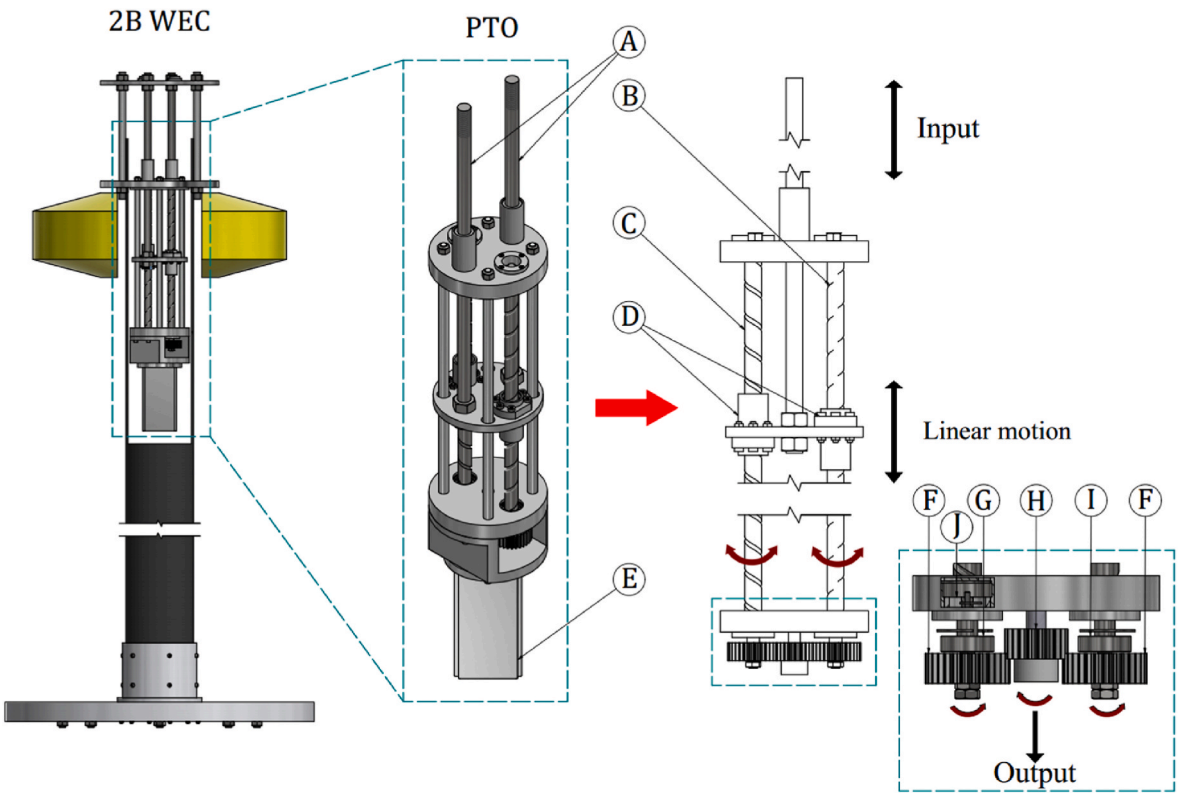

Fig. 2. Two-body point absorber with the rectified unidirectional rotary PTO. A: Connecting rods, B: Right-handed ball screw, C: Left-handed ball screw, D: Ball screw nuts, E: DC generator, F: N30 simple gear, G: One-way bearing (left-handed), H: N22 simple gear, I: One-way bearing (right-handed), J: Deep grove ball bearing.

right-handed thread. The rotational motion of the ball screws is eventually transmitted to the gears (F). The gears are connected to the ball screws by one-way bearings (G and I) which are only allowed to follow the motion of the ball screws in one direction while they are free to rotate idly in the other direction. The one-way bearings are mounted in such a way that they operate in opposite directions, which means that one transfers the clockwise and the other one transfers the counter-clockwise motions. The gear (H), which is driven by the gears (F), is connected to the generator (E) shaft and rotates the generator.

To clarify the mechanism used to have an uni-directional output rotational motion, Fig. 3 is presented. When the floating and submerged bodies move away from each other, the input rod and, consequently, the

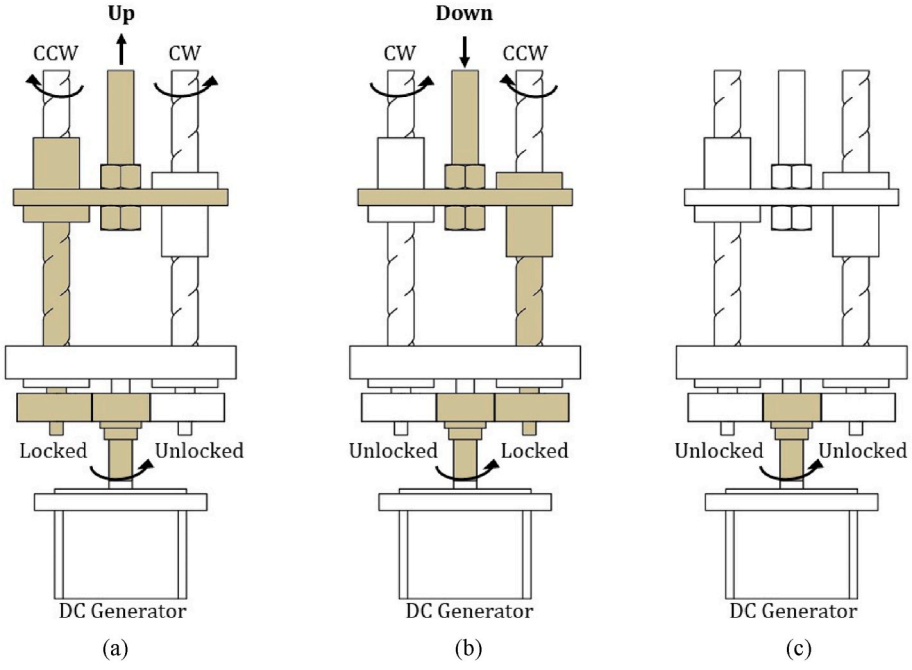

Fig. 3. The uni-directional mechanism of the PTO performance.

ball screw nuts move upwards. Due to the right and left-hand threads of the right and left ball screw nuts, respectively, they rotate clockwise and counterclockwise. As previously mentioned, the ball screw nuts are connected to simple gears through one-way bearings. The bearings are locked counterclockwise and free to rotate clockwise. When the bearing is locked, the rotation of the ball screw can be transferred to the generator shaft gear. Therefore, in the upward movement (Fig. 3 – a), the locked left ball screw can rotate the generator shaft gear in the clockwise direction, while the unlocked right gear can not transfer the ball screw rotation to the generator shaft gear. In the downward movement (Fig. 3 – b), a similar process occurs for the locked right ball screw nut, and the generator shaft rotates again in the clockwise direction. It means that the generator shaft always rotates in the clockwise direction.

When the generator is rotated by the ball screws, it experiences acceleration due to the rotational momentum of internal components. If the rotational speed of the ball screws decreases, the generator still tends to rotate due to its inertia. Using one-way bearings allows the generator to continue its motion with its own inertial momentum, making its rotation independent of the ball screw rotation (Fig. 3 – c). This separation continues until the rotational speed of the ball screws exceeds the generator's rotational speed. Generally speaking, the PTO mechanism works similar to the pedaling mechanism of a bicycle. When a rider pedals the bicycle, the rotational motion of pedaling is transferred to the wheels, causing acceleration and movement of the bicycle. However, if the rider stops pedaling or reduces the speed of pedaling, the bicycle continues to move forward with its own inertia regardless of the pedaling speed.

3. Dynamics

3.1. PTO dynamics

The PTO converts the relative linear motion of the bodies into rotational motion and delivers it to the generator. To develop the dynamic equations of the designed PTO and to calculate the amount of electrical absorbed power, as Fig. 4 shows, consider the force f_{PTO} that the relative motion of bodies inserts in the PTO. The axial force f_m moves the ball screw nuts and connecting rods. The rotational torque T_m rotates ball screws, gears, and bearings. The rotation of the ball screw shaft is transferred to the generator shaft by a gear system. The rotational moment created in the generator shaft is denoted by T_{gen}. The relative displacement dx_{rel} is supposed to occur at time step dt. The linear motion of the ball screw nuts leads to a ball screw rotation of ($d\theta_{bs}$) and a generator shaft rotation of ($d\theta_{gen}$). Considering the principle of energy conservation, the governing equation of the PTO, when the gears are engaged, is written as:

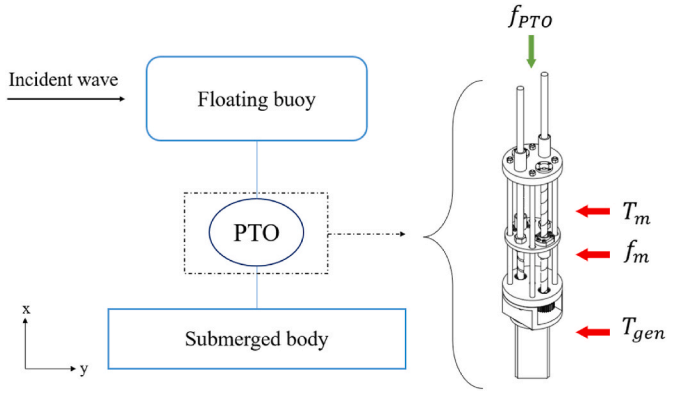

Fig. 4. The rectified unidirectional PTO.

$$f_{PTO}(t)dx_{rel} = \frac{1}{\eta_m}\left(T_m(t)d\theta_{bs} + f_m(t)dx_{rel}\right) + \frac{1}{\eta_e}T_{gen}(t)d\theta_{gen} \quad (1)$$

in which, $T_m(t)$ is the sum of the torques of the ball screw $T_{bs}(t)$ and gears $T_{gears}(t)$, *i.e.*:

$$T_m(t) = T_{bs}(t) + T_{gears}(t) \quad (2)$$

η_m and η_e represent the mechanical and electrical efficiency of the PTO, respectively.

Considering the ball screw pitch (l) and the gears conversion ratio (n), the relationship between the rotational displacement of the ball screw ($d\theta_{bs}$), the rotational displacement of the shaft of the generator ($d\theta_{gen}$), and the linear displacement of the nut of the ball screw (dx_{rel}) at the time of the gear engagement can be expressed as:

$$d\theta_{bs} = \frac{2\pi}{l}dx_{rel} \quad (3)$$

$$d\theta_{gen} = nd\theta_{bs} = \frac{2\pi n}{l}dx_{rel} \quad (4)$$

Substituting Eqs. (3) and (4) into Eq. (1), f_{PTO} can be obtained as:

$$f_{PTO}(t) = \frac{2\pi}{l}\left[\frac{1}{\eta_m}T_m(t) + \frac{n}{\eta_e}T_{gen}(t)\right] + \frac{1}{\eta_m}f_m(t) \quad (5)$$

To calculate f_{PTO} using Eq. (5), we need to find suitable expressions for T_m, T_{gen}, and f_m. In the rest of this section, we will explain how to obtain these expressions.

The torque of the ball screw, $T_{bs}(t)$, only originated from the rotational acceleration of its components, i.e. two ball screw nuts, four bearings, and two one-way bearings:

$$T_{bs}(t) = (2J_{bs} + 4J_b + 2J_{ob})\ddot{\theta}_{bs}(t) = J_m\ddot{\theta}_{bs}(t) \quad (6)$$

in which, $\ddot{\theta}_{bs}$ is the rotational acceleration of the ball screws and J is the moment of inertia. The other notations used in this equation, and the equations that will be presented later, together with their values, are listed in Table 1.

On the other hand, the torque of the gears, T_{gears}, including two driver gears and one driven gear, can be calculated as:

$$T_{gears}(t) = 2J_{gear_{bs}}\ddot{\theta}_{bs}(t) + J_{gear_{gen}}\ddot{\theta}_{gen}(t) \quad (7)$$

It should be noted that, since the driver gears are connected to the ball screws, they rotate with the angular velocity of the ball screws, while the driven gear rotates with the angular velocity of the generator shaft.

The rotational accelerations of the generator shaft and the ball screw shafts are related by:

$$\ddot{\theta}_{gen}(t) = n\ddot{\theta}_{bs}(t) \quad (8)$$

Table 1
Specified parameters of the rectified unidirectional PTO.

Physical expression	Symbol	Value
Mass of connecting rod	m_{rod}	740 g
Mass of ball screw nut	m_{bn}	400 g
Lead of ball screw	l	20 mm
Ball screw moment of inertia	J_{bs}	$1.64 \times 10^{-5} kg.m^2$
Deep grove ball bearing moment of inertia	J_b	$4.7 \times 10^{-6} kg.m^2$
One-way bearing moment of inertia	J_{ob}	$1.7 \times 10^{-6} kg.m^2$
Driver gear moment of inertia	$J_{gear_{bs}}$	$4.4 \times 10^{-5} kg.m^2$
Driven gear moment of inertia	$J_{gear_{gen}}$	$1.9 \times 10^{-5} kg.m^2$
Generator moment of inertia	J_{gen}	$3.5 \times 10^{-4} kg.m^2$
Generator torque constant	K_t	0.17 $N.m/A$
Generator electric constant	K_e	0.15 $V.s/rad$
Generator internal resistance	R_{in}	1 Ω
Gear ratio	n	1.36

Substituting Eq. (8) into Eq. (7), results in:

$$T_{gears}(t) = \left[2J_{gear_{bs}} + nJ_{gear_{gen}}\right] \ddot{\theta}_{bs}(t) = J_{gears}\, \ddot{\theta}_{bs}(t) \tag{9}$$

T_m can be obtained by, substituting Eqs. (6) and (9) into Eq. (2), as:

$$T_m(t) = \left(J_m + J_{gears}\right)\ddot{\theta}_{bs}(t) \tag{10}$$

To obtain an expression for T_{gen}, the second term in Eq. (2), we can divide it into mechanical parts, $T_{m_{gen}}$, and electrical parts, $T_{e_{gen}}$. The mechanical torque, which refers to the stator and rotational components, is represented by:

$$T_{m_{gen}}(t) = J_{gen}\ddot{\theta}_{gen}(t) \tag{11}$$

The electrical torque of the generator, on the other hand, is proportional to the output current, *i.e.:*

$$T_{e_{gen}}(t) = K_t i_{gen}(t) \tag{12}$$

in which K_t is the torque constant and i_{gen} is the output current of the DC generator.

The generator voltage, $v_e(t)$, is related to the rotational speed, $\dot{\theta}_{gen}(t)$, by the following equation:

$$v_e(t) = K_e \dot{\theta}_{gen}(t) \tag{13}$$

in which K_e is the electric constant of the generator.

Using Ohm's law, $v_e(t) = i_{gen}(t).R$, the electrical torque of the generator can be calculated as:

$$T_{e_{gen}}(t) = \frac{K_t K_e}{R}\dot{\theta}_{gen}(t) = \left(\frac{K_t K_e}{R_{in} + R_{ex}}\right)\dot{\theta}_{gen}(t) \tag{14}$$

in which the electrical resistance R is divided into internal, R_{in}, and external resistances, R_{ex}, (external resistance plays the role of external load, and it changes based on the electric current consumption). Eq. (14) can be written as:

$$T_{e_{gen}}(t) = c_{gen}\dot{\theta}_{gen}(t) \tag{15}$$

in which c_{gen} is the damping coefficient of the generator, expressed in Eq. (16).

$$c_{gen} = \left(\frac{K_t K_e}{R_{in} + R_{ex}}\right) \tag{16}$$

Considering Eqs. (11) and (15), $T_{gen}(t)$ can be expressed as:

$$T_{gen}(t) = J_{gen}\ddot{\theta}_{gen}(t) + c_{gen}\dot{\theta}_{gen}(t) \tag{17}$$

To obtain an expression for the third term f_m in Eq. (5), we can write the following expression:

$$f_m(t) = (m_{bn} + m_{rod})\ddot{x}_{rel}(t) = m_p\ddot{x}_{rel}(t) \tag{18}$$

where $\ddot{x}_{rel}(t)$ is the relative acceleration of the bodies. This equation states that the force applied by the WEC bodies on the PTO by rods (A), as shown in Fig. 2, is spent to accelerate the masses of these rods together with those of ball screw nuts.

By substituting Eqs. (10), (17) and (18) into Eq. (5), the PTO force, $f_{PTO_{eng}}$, when the generator is engaged with the rectifying system, can be obtained as follows:

$$f_{PTO_{eng}}(t) = \frac{2\pi}{l}\left[\frac{1}{\eta_m}\left[J_m + J_{gears}\right]\ddot{\theta}_{bs}(t) + \frac{n}{\eta_e}\left[J_{gen}\ddot{\theta}_{gen}(t) + c_{gen}\dot{\theta}_{gen}(t)\right]\right] + \frac{1}{\eta_m}m_p\ddot{x}_{rel}(t) \tag{19}$$

By replacing $\ddot{\theta}_{bs}(t) = \frac{2\pi}{l}\ddot{x}_{rel}(t)$, $\ddot{\theta}_{gen}(t) = \frac{2\pi n}{l}\ddot{x}_{rel}(t)$, and $\dot{\theta}_{gen}(t) = \frac{2\pi n}{l}\dot{x}_{rel}(t)$ in the above equation, Eq. (19) can be written as:

$$f_{PTO_{eng}}(t) = m_{eng}\ddot{x}_{rel}(t) + c_{eng}\dot{x}_{rel}(t) \tag{20}$$

in which m_{eng} and c_{eng} are defined as:

$$m_{eng} = \left(\frac{2\pi}{l}\right)^2\left[\frac{1}{\eta_m}\left[J_m + J_{gears}\right] + \frac{n^2}{\eta_e}J_{gen}\right] + \frac{1}{\eta_m}m_p \tag{21}$$

$$c_{eng} = \left(\frac{2\pi n}{l}\right)^2\frac{1}{\eta_e}c_{gen} \tag{22}$$

Eq. (20) relates the PTO force to the relative linear acceleration and velocity in the time domain. To transfer Eq. (20) into the frequency domain, we consider the linear relative velocity as $\dot{x}_{rel}(t) = Re\{\widehat{U}_{rel}e^{i\omega t}\}$ and the PTO force as $f_{PTO_{eng}}(t) = Re\{\widehat{F}_{PTO_{eng}}e^{i\omega t}\}$, in which $\widehat{U}_{rel}$ is the complex amplitude of the relative velocity and $\widehat{F}_{PTO_{eng}}$ is the complex amplitude of the PTO force. Replacing these relations into Eq. (20), the PTO forces in the frequency domain can be obtained as:

$$\widehat{F}_{PTO_{eng}} = \left(i\omega m_{eng} + c_{eng}\right)\widehat{U}_{rel} = Z_{PTO_{eng}}\widehat{U}_{rel} \tag{23}$$

where,

$$Z_{PTO_{eng}} = i\omega m_{eng} + c_{eng} \tag{24}$$

in which Z_{PTO} is the complex impedance of the PTO.

A regular wave with a sinusoidal motion creates a sinusoidal relative velocity $\dot{x}_{rel}$ in the heave direction. Therefore, by taking the derivative of Eq. (3), one can conclude that the ball screw angular velocity can be obtained as $\dot{\theta}_{bs} = \dot{\theta}_0|\sin(\omega t)|$ as indicated by the dashed line in Fig. 5, in which $\dot{\theta}_0$ is the amplitude of angular velocity. As the ball screw approaches its final position, its angular speed approaches zero, while the generator shaft continues to rotate due to its rotational inertia. When the angular speed of the generator shaft $\dot{\theta}_{gen}$ exceeds the angular speed of the ball screw shaft ($\dot{\theta}_{gen_{dis}}(t) > \dot{\theta}_{gen_{eng}}(t)$), disengagement occurs. In this case, no external torque is applied to the generator shaft. Therefore, the equation of motion of the generator during the disengagement time can be written as:

$$J_{gen}\ddot{\theta}_{gen_{dis}}(t) + c_{gen}\dot{\theta}_{gen_{dis}}(t) = 0 \tag{25}$$

If we consider that the ball screw and generator disengagement occurs at t_d and engage again at t_e, then:

$$\dot{\theta}_{gen_{dis}}(t) = e^{-k\Delta t}\dot{\theta}_{gen}(t_d) \tag{26}$$

in which $k = \frac{c_{gen}}{J_{gen}}$.

The disengagement conditions can be expressed mathematically as:

$$e^{-k\Delta t}\sin(\omega t_d) > \sin(\omega(t_d + \Delta t)) \tag{27}$$

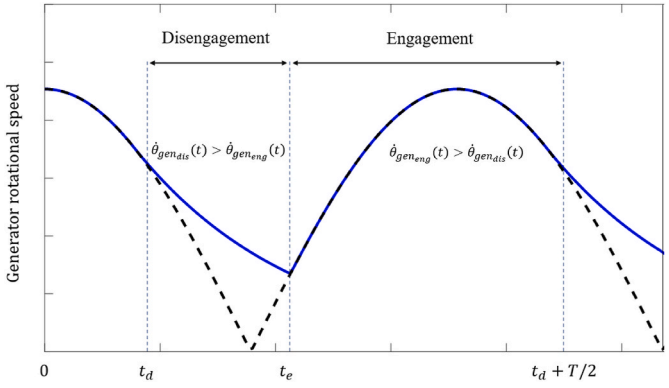

Fig. 5. Simulation results of the generator rotational speed for the rectified unidirectional PTO.

where Δt is a time interval shortly after the disengagement.

When $\dot{\theta}_{gen_{dis}}(t) < \dot{\theta}_{gen_{eng}}(t)$, the generator shaft is engaged again. Shortly after re-engagement,

$$e^{-k\Delta t}\sin(\omega t_e) < \sin(\omega(t_e+\Delta t)) \tag{28}$$

Fig. 5 compares the angular speed of the generator shaft with that of the ball screw shaft, as a function of time. As indicated in this figure, between time t_d and t_e, the inertia of the generator overcomes the ball screws' rotating velocity and the generator rotates with the velocity given in Eq. (26). Once the ball screw velocity increases, the generator shaft connects to the ball screw and rotates at $\dot{\theta}_{bs}$ (t). Eqs. (27) and (28) can be solved numerically to determine the times at which disengagement (t_d) and engagement (t_e) occur.

3.2. WEC dynamics

Fig. 9 shows a 2B-PA modeled as a 2-DoF mass-spring-damper system. Based on the linear wave theory, the frequency domain equation of motion for a 2B-PA that oscillates in the heave direction can be written as (Falnes, 1999):

$$Z(\omega)[\widehat{U}_1\ \widehat{U}_2]^T = \begin{bmatrix} Z_1+Z_{PTO} & -Z_{PTO} \\ -Z_{PTO} & Z_2+Z_{PTO} \end{bmatrix}[\widehat{U}_1\ \widehat{U}_2]^T = [\widehat{F}_{e_1}\ \widehat{F}_{e_2}]^T \tag{29}$$

where $\widehat{U}_j$ $(j=1.2)$ is the complex amplitude of each body velocity (subscripts 1 and 2 refer to the floating and submerged bodies, respectively). $\widehat{F}_{e_j}$ is the complex frequency-dependent wave excitation force. $Z(\omega)$ is the complex mechanical impedance matrix, in which:

$$Z_1 = (B_1 + b_{vis1}) + i\omega\left(m_1 + A_1 - \frac{K_{s1}}{\omega^2}\right) \tag{30}$$

$$Z_2 = (B_2 + b_{vis2}) + i\omega\left(m_2 + A_2 - \frac{K_{s2}}{\omega^2}\right) \tag{31}$$

where B_j, A_j, K_{sj} are the frequency-dependent radiation damping, added mass, and hydrostatic stiffness coefficients, respectively. b_{visj} is the viscous damping coefficients, m_j is the physical mass of each body, i is the imaginary unit, and ω [rad/s] is the wave frequency. Z_{PTO} is the complex mechanical impedance induced by the load of the PTO, which can be obtained by Eq. (24). The frequency-dependent coefficients can be extracted by the frequency domain BEM solver, ANSYS-AQWA (ANSYS Inc, 2017), or by experiments in a wave tank. Viscous damping coefficients can be obtained either by CFD simulations or by radiation tests. In ref. (Rahimi et al., 2022), the hydrodynamic characteristics of the WEC are calculated and compared, using numerical, analytical and experimental methods. Added mass, damping coefficient, and normalized excitation force values, for floating and submerged bodies are illustrated in Figs. 6–8, respectively.

From Eq. (29), the relative velocity of the two bodies can be obtained as

$$\widehat{U}_{rel} = \widehat{U}_1 - \widehat{U}_2 = \frac{\frac{\widehat{F}_{e1}Z_2 - \widehat{F}_{e2}Z_1}{(Z_1+Z_2)}}{\frac{Z_1Z_2}{(Z_1+Z_2)} + Z_{PTO}} = \frac{\widehat{F}_{eq}}{Z_{eq}+Z_{PTO}} \tag{32}$$

where $\widehat{F}_{eq}$ and Z_{eq} are the equivalent wave excitation force and the equivalent complex mechanical impedance matrix, respectively, defined as

$$\widehat{F}_{eq} = \frac{\widehat{F}_{e1}Z_2 - \widehat{F}_{e2}Z_1}{(Z_1+Z_2)} \tag{33}$$

$$Z_{eq} = \frac{Z_1Z_2}{(Z_1+Z_2)} \tag{34}$$

Using Eqs. (3), (22), (24), and (32), the angular speed of the generator can be obtained as:

$$\begin{aligned}\widehat{\dot{\theta}}_{gen} &= \frac{2\pi n}{l}\widehat{U}_{rel} = \left(\frac{2\pi n}{l}\right)\frac{\widehat{F}_{eq}}{Z_{eq}+Z_{PTO}} \\ &= \left(\frac{2\pi n}{l}\right)\frac{\widehat{F}_{eq}}{\left(Re\{Z_{eq}\} + \left(\frac{2\pi n}{l}\right)^2\frac{1}{\eta_e}c_{gen}\right) + i\left(Im\{Z_{eq}\} + \omega m_{eng}\right)}\end{aligned} \tag{35}$$

4. Power absorption and optimal condition

In this section, the electrical average power generated by the PTO for both the rectified and bidirectional PTO will be compared.

4.1. Rectified unidirectional PTO

The electrical averaged absorbed power of a unidirectional PTO, denoted by P_{E-uni}, can be calculated using Eq. (36):

$$P_{E-uni} = \frac{2}{T}\left[\int_{t_d}^{t_e} T_{e_{gen}}(t)\dot{\theta}_{gen_{dis}}(t)dt + \int_{t_e}^{t_d+\frac{T}{2}} T_{e_{gen}}(t)\dot{\theta}_{gen_{eng}}(t)dt\right] \tag{36}$$

in which $\dot{\theta}_{gen_{dis}}$ and $\dot{\theta}_{gen_{eng}}$ can be obtained from Fig. 5.

Replacing $T_{e_{gen}}(t)$ from Eq. (15) in the above equation results in:

$$P_{E-uni} = \frac{2}{T}\left[\int_{t_d}^{t_e} c_{gen}\dot{\theta}^2_{gen_{dis}}(t)dt + \int_{t_e}^{t_d+\frac{T}{2}} c_{gen}\dot{\theta}^2_{gen_{eng}}(t)dt\right] \tag{37}$$

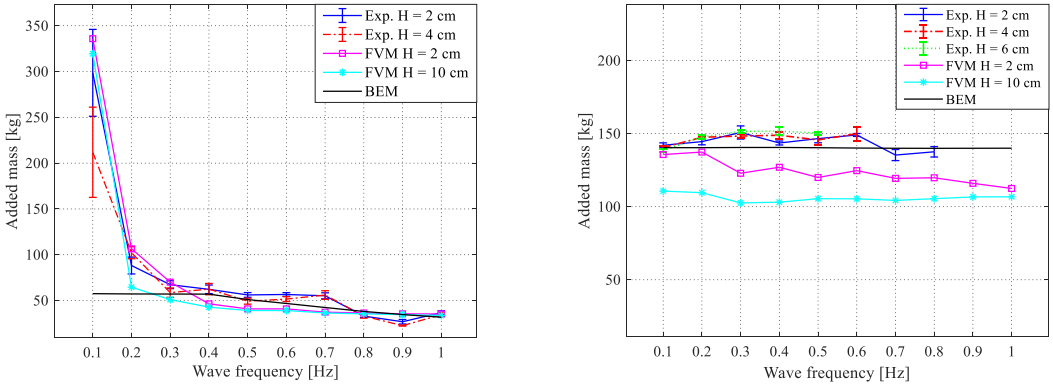

Fig. 6. Added mass for (a) the floating and (b) submerged bodies (Rahimi et al., 2022).

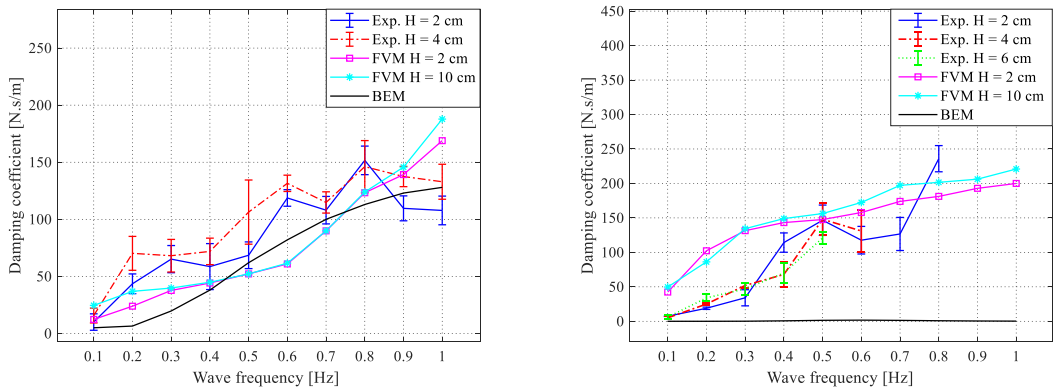

Fig. 7. Damping coefficient for (a) the floating buoy and (b) submerged bodies (Rahimi et al., 2022).

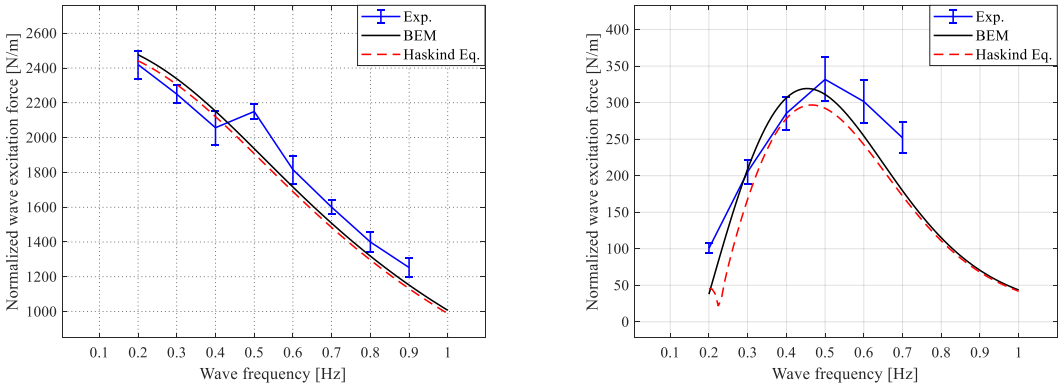

Fig. 8. Normalized wave excitation force acting on (a) the floating and (b) the submerged bodies. (The force is normalized by the wave height, η) (Rahimi et al., 2022).

Because t_e and t_d are found numerically, Eq. (37) cannot be solved analytically. Eq. (37) can be discretized using the trapezoidal rule as:

$$P_{E-uni} = \frac{2}{T}\left\{\sum_{j=0}^{n} c_{gen}\dot{\theta}^2_{gen_{dis}}(t_j)\Delta t \quad t_d < t_j < t_e\right\} + \frac{2}{T}\left\{\sum_{j=n+1}^{m} c_{gen}\dot{\theta}^2_{gen_{eng}}(t_j)\Delta t \quad t_e < t_j < t_d + \frac{T}{2}\right\} \tag{38}$$

By choosing proper damping for the generator (c_{gen}), the maximum electrical power can be obtained. In Eq. (38), both the generator damping coefficient and generator angular speed ($\dot{\theta}_{gen_{eng}}$; $\dot{\theta}_{gen_{dis}}$) depend on the external resistance of the generator. In other words, the external resistance directly changes c_{gen}, according to Eq. (16). Then, c_{gen} changes the generator angular velocity by affecting the mechanical impedance of the PTO in Eq. (24), $\widehat{\dot{\theta}}_{gen}$ in Eq. (35), and k coefficient in Eq. (26). To find the optimal value of R_{ex} at each frequency, the range of external resistance is chosen to be 1–30 Ohm, and Eq. (38) is solved by iterating in the selected range with a 0.1 Ω interval. Then, the maximum electrical power and its associated external resistance can be calculated.

4.2. Bidirectional PTO

If the PTO is bidirectional, the rotation direction of the generator changes as the direction of the relative velocity changes. The electrical average absorbed power for a 2B WEC with a bidirectional PTO, denoted by P_{E-Bi}, can be shown to be

$$P_{E-Bi} \equiv \overline{p_E(t)} = \frac{2}{T}\int_0^{\frac{T}{2}} c_{gen}\dot{\theta}_{gen}{}^2(t)dt = \frac{1}{2}c_{gen}\left|\widehat{\dot{\theta}}_{gen}\right|^2 \tag{39}$$

Replacing Eq. (35) into Eq. (39) results in the following equation for the average absorbed power of a bidirectional PTO:

$$P_{E-Bi} = \frac{1}{2}c_{gen}\left(\frac{2\pi n}{l}\right)^2\left|\frac{\widehat{F}_{eq}}{\left(Re\{Z_{eq}\} + \left(\frac{2\pi n}{l}\right)^2\frac{1}{\eta_e}c_{gen}\right) + i\left(Im\{Z_{eq}\} + \omega m_{eng}\right)}\right|^2 \tag{40}$$

As indicated in this equation, the electrical absorbed power can be altered by changing c_{eng}. To obtain the optimum c_{eng}, which maximizes the absorbed power, the partial derivative of P_{E-Bi} with respect to c_{eng} must be set equal to zero, *i.e.:*

$$\frac{\partial P_{E-Bi}}{\partial c_{gen}} = 0 \tag{41}$$

This results in:

$$c_{gen_{opt}} = \eta_e\left(\frac{l}{2\pi n}\right)^2\sqrt{\left(Re\{Z_{eq}\}\right)^2 + \left(Im\{Z_{eq}\} + \omega m_{eng}\right)^2} \tag{42}$$

Using Eq. (16), the external resistance R_{ex} can be adjusted to achieve the optimum generator damping coefficient as:

$$R_{ex_{opt}} = \frac{K_t K_e}{c_{gen_{opt}}} - R_{in} \tag{43}$$

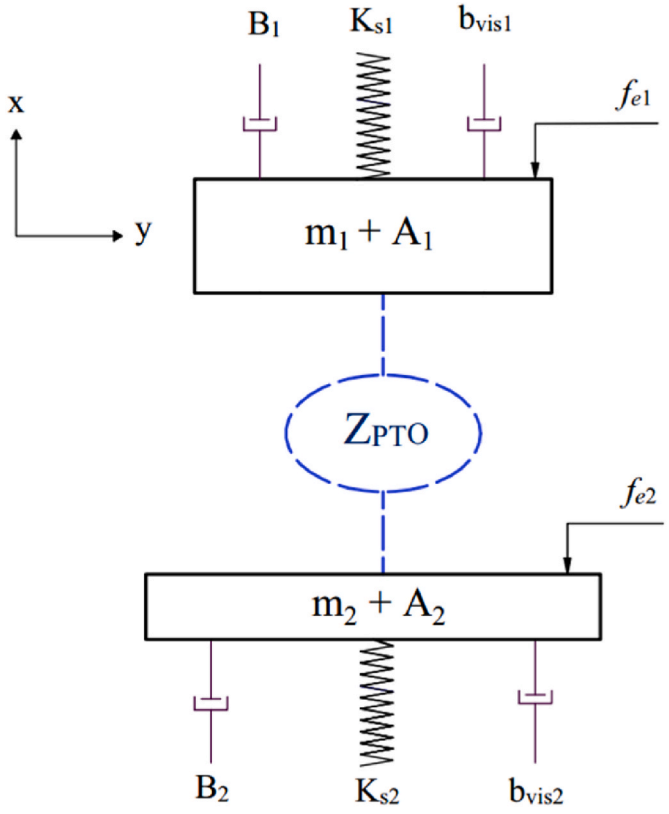

Fig. 9. 2-DOF mass-spring-damper model of the 2B-PA.

5. Results

5.1. Disengagement ratio

As discussed in Section 3.1 and shown in Fig. 5, in a part of a rotation period, the generator disengages from the ball screw gear and rotates independently due to the inertia of the generator shaft. This means that at the disengagement time ($t_e - t_d$) the generator shaft rotates faster than the ball screw gear. The angular velocity of the generator shaft is the output rotating speed. Therefore, the efficiency of the absorbed power increases as the disengagement time increases. Fig. 10 shows the disengagement ratio, defined as the ratio of the disengagement time to the rotation period of the PTO, at various frequencies in the range of 0.2–1 Hz. As shown in this figure, the shortest disengagement time occurs around the frequency of 0.5 Hz. When the frequency increases to about 0.7 Hz, the disengagement time increases, and it drops again at frequencies higher than 0,8 Hz. This indicates that the rectified unidirectional PTO is most efficient at frequencies around 0.7–1 Hz. Since the disengagement ratio at frequencies near 0.5 Hz is low, the performance of the unidirectional PTO is not much better than the bidirectional PTO. This hypothesis is examined in the following sections, and is used to determine the efficiency of the mechanism at different frequencies.

5.2. Optimal condition

One way to increase the power absorbed by the WEC is to optimize the PTO generator damping coefficient. As discussed in Section 4, the optimal condition can be achieved by changing the damping coefficient of the PTO generator c_{gen} in Eq. (16) by changing its external resistance at each wave frequency, for both uni- and bidirectional PTOs. The optimal external resistance is calculated numerically and analytically based on Eqs. (38) and (43) for uni- and bidirectional PTOs, respectively. Fig. 11 illustrates the optimal external resistance in the frequency range of 0.2–1 Hz, for both types of PTOs. The optimum external resistance of the generator, shown in Fig. 11, and the normalized electrical averaged absorbed power, shown in Fig. 12, are calculated using the values listed in Table 1 as well as the hydrodynamic coefficients and wave excitation forces presented in (Rahimi et al., submitted). For frequencies smaller than 0.6 Hz, the unidirectional and the bidirectional optimal resistances are almost identical. When the frequency exceeds 0.6 Hz, the optimal values of unidirectional resistance appear to be higher than those of bidirectional resistance. The maximum difference between the resistances occurs in the frequency range of 0.8–1 Hz. This is in agreement with the variation of the disengagement ratio with wave frequency, shown in Fig. 10, in which the maximum disengagement ratio occurs in the frequency range of 0.8–1 Hz as well.

In the next step, the electrical average absorbed power using the optimal external resistance will be calculated.

5.2. Power absorption

Fig. 12 shows the electrical absorbed power of the two-body WEC with the uni- and bidirectional PTO in the frequency range of 0.2–1 Hz, obtained by solving Eqs. (38) and (40), respectively. The powers are calculated for optimum generator damping resistance, obtained by using the optimal external resistances, shown in Fig. 11. The following results

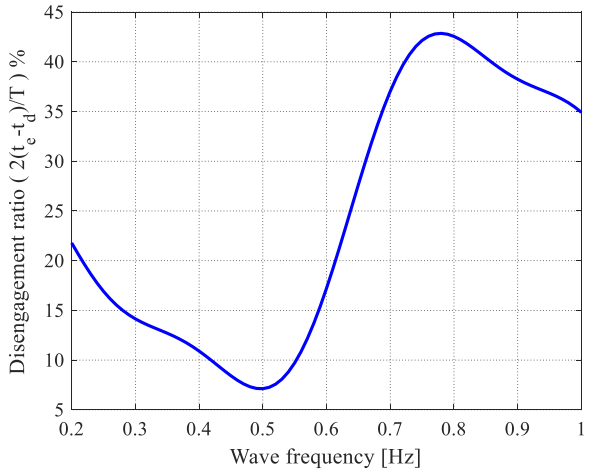

Fig. 10. Disengagement ratio as a function of wave frequency defined as $2\frac{t_e - t_d}{T} \times 100$.

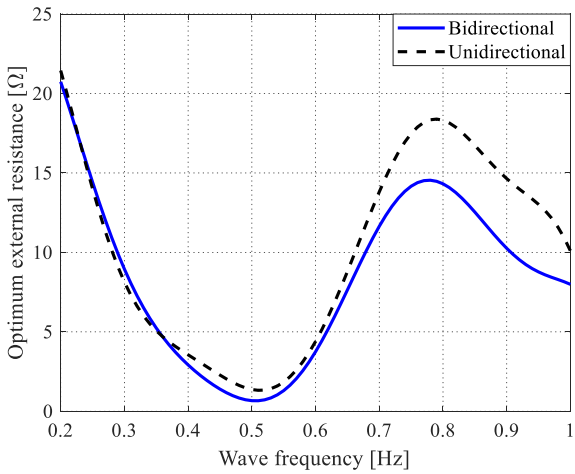

Fig. 11. Optimal external resistance of the generator.

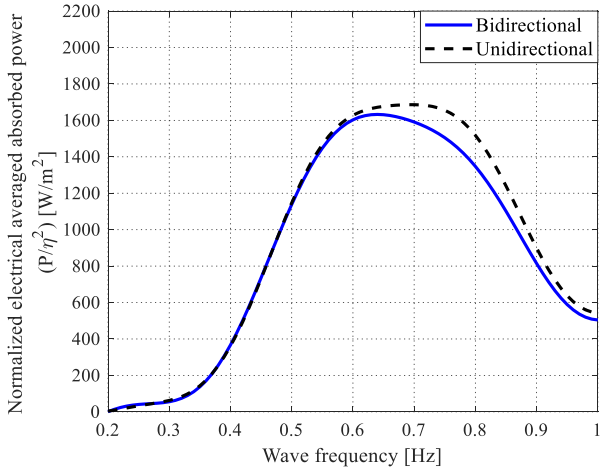

Fig. 12. Normalized electrical averaged absorbed power for uni- and bidirectional PTO.

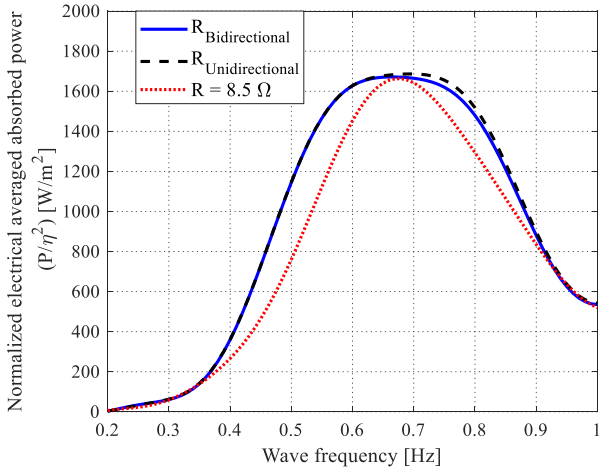

Fig. 14. Normalized electrical averaged absorbed power for three different *R*.

are extracted from Fig. 12: (i) the electrical average absorbed power increases when the unidirectional PTO is used. For the specified WEC mentioned in Section 3.2, the unidirectional PTO converts 9% more power than the bidirectional PTO in the frequency range of 0.7–1 Hz. (ii) For frequencies less than 0.6 Hz, both the uni- and the bidirectional PTO have the same power output. At frequencies less than 0.6 Hz, the disengagement time is not significant and both mechanisms operate similarly. In other words, the unidirectional PTO works more efficiently for frequencies above 0.8 Hz. Fig. 13 depicts the percentage of the increase in electrical power efficiency ($\frac{P_{E-Uni}-P_{E-Bi}}{P_{E-Bi}} \times 100$) when the unidirectional PTO is used, relative to the corresponding values of the bidirectional PTO. The maximum increase is 13% and occurs around the frequency of 0.75 Hz. Fig. 14 shows the absorbed electrical power of the WEC with a bidirectional and a unidirectional PTO with variable optimal R in blue and black dash lines, respectively, and with a fixed R-value in the red line.

It has already been discussed that one option to reach the maximum power is to choose the optimum external resistance at each frequency. A mathematical model is presented for the bidirectional PTO – to suggest the optimal external resistance based on the wave frequency. The numerical solution of Eq. (38) offers the optimal values of external resistances for the unidirectional PTO. This section tries to introduce a mathematical model for the optimal resistance of the unidirectional PTO, since having an analytical relation between the optimal resistance and wave frequency is more useful than the numerical calculations in control algorithms. One option is to consider the bidirectional PTO optimal resistance (Eq. (43)) as an alternative for the unidirectional PTO optimal condition. The other option is to choose a fixed external resistance at all frequencies. Fig. 14 compares the electrical absorbed power of the unidirectional PTO for the external resistances obtained from numerical solution (Eq. (38)) with the corresponding values obtained for the bidirectional PTO, as well as the absorbed power when a fixed external resistance is used for all frequencies. To calculate a fixed value for the external resistance, it is assumed that the probability of the wave incident at each frequency in the range of 0.2–1 Hz is the same. The optimal fixed value is chosen to maximize the averaged absorbed power in the mentioned frequency range. For the designed PTO and WEC specification, the optimal fixed value of external resistance is 8.8 Ω. The average absorbed power for the optimal unidirectional PTO and for the fixed resistance PTO in the range of 0.2–1 Hz are 990 W/m^2 and 750 W/m^2, respectively.

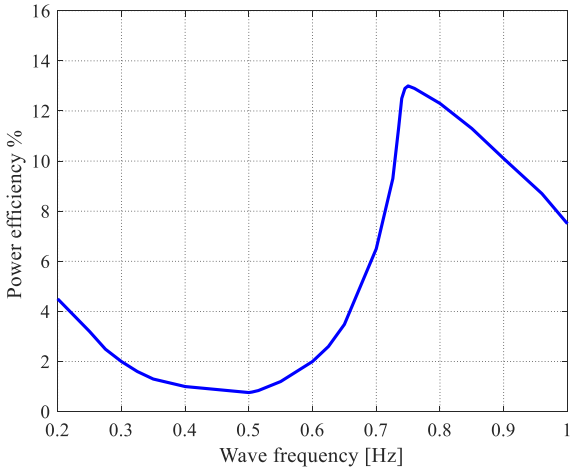

Fig. 13. Power efficiency, $\frac{P_{E-Uni}-P_{E-Bi}}{P_{E-Bi}} \times 100$.

6. Conclusions

The aim of this study is to design and analyze the performance of a PTO which can convert the relative velocity of the two bodies of a WEC into a unidirectional non-stop rotational motion. A new mechanism is introduced which benefits from the ball screw and nut system to convert the linear into one-directional rotary motion. Using a one-way bearing and gear system, the PTO is able to couple and decouple the generator to the relative velocity of the bodies. Once the inertia of the generator causes the generator shaft to continue to rotate independently of the ball screw angular velocity, disengagement occurs and the generator rotates faster than the ball screw. The study is concluded as below.

- The results of this study reveal that rectifying the unidirectional PTO (engagement/disengagement mechanism) generates 9% more electrical power than the simple bidirectional PTO in the frequency range of 0.7–1 Hz.
- Generator external resistance is used as a control parameter for the PTO. Depending on the incident wave frequency, this parameter is adjusted to maximize the absorbed power. As an alternative for the variable external resistance, a fixed value can be taken to maximize the average absorbed power in a frequency domain.
- The benefit of the linear ball screw and nut system in the rectified PTO is that it helps to reduce the mechanical friction. Since the nut is in contact with the ball screw through the balls, the friction is converted into rolling friction.

- Based on the obtained results, rectifying the PTO does not enhance the PTO performance at low frequencies.

CRediT authorship contribution statement

Saeed Rezaei: Conceptualization, Methodology, Software, Validation, Writing – original draft. **Amir Rahimi:** Conceptualization, Investigation, Visualization, Validation, Writing – original draft. **Jamshid Parvizian:** Project administration, Writing – review & editing, Funding acquisition. **Shahriar Mansoorzadeh:** Supervision, Writing – review & editing, Validation. **Alexander Düster:** Project administration, Writing – review & editing, Funding acquisition.

Declaration of competing interest

The authors declare that they have no known competing financial interests or personal relationships that could have appeared to influence the work reported in this paper.

Data availability

Data will be made available on request.

Acknowledgment

This work is the result of an institutional partnership supported by the Alexander von Humboldt Foundation. This support is gratefully acknowledged.

References

Al, SHami, et al., 2019a. A parameter study and optimization of two body wave energy converters. Renew. Energy 131, 1–13.
Al, Shami, et al., 2019b. Point absorber wave energy harvesters: a review of recent developments. Energies 12, 47.
ANSYS Inc, 2017. AQWA Theory Manual. Canonsburg, PA 15317.
António, F.D.O., 2007. Modelling and control of oscillating-body wave energy converters with hydraulic power take-off and gas accumulator. Ocean. Eng. 34, 2021–2032.
Babarit, A., Clement, A.H., 2006. Optimal latching control of a wave energy device in regular and irregular waves. Appl. Ocean Res. 28, 77–91.
Babarit, A., et al., 2009. Declutching control of a wave energy converter. Ocean. Eng. 36, 1015–1024.
Beatty, S.J., et al., 2015. Experimental and numerical comparisons of self-reacting point absorber wave energy converters in regular waves. Ocean. Eng. 104, 370–386.
Bozzi, S., et al., 2013. Wave energy production in Italian offshore: preliminary design of a point absorber with tubular linear generator. In: 4th International Conference on Clean Electrical Power: Renewable Energy Resources Impact, ICCEP, pp. 203–208. https://doi.org/10.1109/ICCEP.2013.6586990, 2013, art. no. 6586990.
Brekken, T.K., et al., 2009. Ocean wave energy overview and research at Oregon State University. IEEE Power Electron. Mach. W. Appl. 1–7.
Cargo, C.J., et al., 2012. Determination of optimal parameters for a hydraulic power take-off unit of a wave energy converter in regular waves. Proc. Inst. Mech. Eng. A J. Power Energy 226, 98–111.
Falcão, A.F.D.O., 2010. Wave energy utilization: a review of the technologies. Renew. Sustain. Energy Rev. 14, 899–918.
Falnes, J., 1999. Wave-energy conversion through relative motion between two single-mode oscillating bodies. J. Offshore Mech. Arctic Eng. 121, 32–38.
Falnes, J., 2007. A review of wave-energy extraction. Mar. Struct. 20, 185–201.
Folley, M., et al., 2007. The design of small seabed-mounted bottom-hinged wave energy converters. In: Proceedings of the 7th European Wave and Tidal Energy Conference, 312. Citeseer.
Goggins, J., Finnegan, W., 2014. Shape optimisation of floating wave energy converters for a specified wave energy spectrum. Renew. Energy 71, 208–220.
Henderson, R., 2006. Design, simulation, and testing of a novel hydraulic power take-off system for the Pelamis wave energy converter. Renew. Energy 31, 271–283.
Hodgins, N., et al., 2011. Design and testing of a linear generator for wave-energy applications. IEEE Trans. Ind. Electron. 59, 2094–2103.
Illesinghe, S., et al., 2017. Idealized design parameters of Wave Energy Converters in a range of ocean wave climates. Int. J. Mar. Energy 19, 55–69.
Khatri, P., Wang, X., 2020. Comprehensive review of a linear electrical generator for ocean wave energy conversion. IET Renew. Power Gener. 14, 949–958.
Kurniawan, A., Moan, T., 2012. Optimal geometries for wave absorbers oscillating about a fixed axis. IEEE J. Ocean. Eng. 38, 117–130.
Leijon, et al., 2008. Wave energy from the north sea: experiences from the Lysekil research site. Surv. Geophys. 29, 221–240.
Li, X., et al., 2020. A compact mechanical power take-off for wave energy converters: design, analysis, and test verification. Appl. Energy 278, 115459.
Liang, C., Zuo, L., 2017. On the dynamics and design of a two-body wave energy converter. Renew. Energy 101, 265–274.
Liang, C., et al., 2017. Design, fabrication, simulation and testing of an ocean wave energy converter with mechanical motion rectifier. Ocean. Eng. 136, 190–200.
Miquel, A.M., et al., 2017. Non-linear modelling of a heaving point absorber: the surge effect. Int. J. Mar. Energy 19, 95–109.
Morim, J., et al., 2014. A review of wave energy estimates for nearshore shelf waters off Australia. Int. J. Mar. Energy 7, 57–70.
Pastor, J., Liu, Y., 2014. Frequency and time domain modeling and power output for a heaving point absorber wave energy converter. Int. J. Mar. Energy Environ. Eng. 5, 1–13.
Polinder, H., et al., 2007. Linear generator systems for wave energy conversion. In: Proceedings of the 7th European Wave and Tidal Energy Conference. IDMEC-Institute de Engenharia Mecânica, Porto.
Prudell, J., et al., 2010. A permanent-magnet tubular linear generator for ocean wave energy conversion. IEEE Trans. Ind. Appl. 46, 2392–2400.
Rahimi, A., et al., 2022. Numerical and experimental study of the hydrodynamic coefficients and power absorption of a two-body point absorber wave energy converter. Renew. Energy 201, 181–193.
Rezaei, S., et al., 2022. Dimensional optimization of a two-body Wave energy converter using response surface methodology. Ocean. Eng. 261, 112186.
Weber, J., et al., 2009. Wavebob—research & Development Network and Tools in the Context of Systems Engineering. Proc. Eighth European Wave and Tidal Energy Conference, Uppsala, Sweden, pp. 416–420.
Weinstein, A., et al., 2004. AquaBuOY-the offshore wave energy converter numerical modeling and optimization. In: Oceans' 04 MTS/IEEE Techno-Ocean'04 (IEEE Cat. No. 04CH37600). IEEE, pp. 1854–1859.
Wen, Y., et al., 2018. A shape optimization method of a specified point absorber wave energy converter for the south China sea. Energies 11, 2645.
Wu, J., et al., 2018. Real-time latching control strategies for the solo Duck wave energy converter in irregular waves. Appl. Energy 222, 717–728.
Yang, Y., et al., 2021. A wave energy harvester based on coaxial mechanical motion rectifier and variable inertia flywheel. Appl. Energy 302, 117528.
Zhang, X.T., et al., 2014. Declutching control of a point absorber with direct linear electric PTO systems. Ocean Syst. Eng. 4, 63–82.
Zurkinden, et al., 2014. Non-linear numerical modeling and experimental testing of a point absorber wave energy converter. Ocean. Eng. 78, 11–21.